ELSEVIER

Journal of the Mechanics and Physics of Solids
52 (2004) 1481–1505

JOURNAL OF THE
MECHANICS AND
PHYSICS OF SOLIDS

www.elsevier.com/locate/jmps

Compressive strength of fibre composites with random fibre waviness

D. Liu, N.A. Fleck*, M.P.F. Sutcliffe

Cambridge University Engineering Department, Trumpington Street, Cambridge, CB2 1PZ, UK

Received 25 November 2003; received in revised form 21 January 2004; accepted 22 January 2004

Abstract

The compressive strength of unidirectional long fibre composites is predicted for plastic microbuckling from a random two-dimensional distribution of fibre waviness. The effect of the physical size of waviness is addressed by using couple stress theory, with the fibre bending resistance scaling with the fibre diameter d. The predicted statistical distribution of compressive strength is found using a Monte Carlo method. An ensemble of fibre waviness profiles is generated from an assumed spectral density of waviness and the compressive strength for each such realisation is calculated directly by the finite element method. The average predicted strength agrees reasonably with practical values, confirming the hypothesis that microbuckles can be initiated by fibre misalignment. It is found that the probability distribution of strength is well matched by a Weibull fit, and the dependence of the Weibull parameters upon the spectral density of waviness is determined. For the practical range of fibre distributions considered, it is concluded that the strength depends mainly upon the root mean square amplitude of fibre misalignment, with the shape of the power spectral density function playing only a minor role. An engineering model for predicting the compressive strength is proposed, akin to weakest link theory for materials containing flaws. A specimen containing randomly distributed waviness is examined to locate regions of high-fibre misalignment. The strength of each of these weak regions is estimated from a look-up table derived from calculations with idealised circular or elliptical patches of waviness. The strength of the composite is given by the failure stress associated with the weakest such patch. For random distributions of waviness, the predictions using this engineering approach are in good agreement with the direct calculations of strength using the finite element method.

Keywords: B, Fibre-reinforced composite material; C, Finite elements; Microbuckling

* Corresponding author. Tel.: +44-1223-332650; fax: +44-1223-332662.
E-mail address: naf1@eng.cam.ac.uk (N.A. Fleck).

0022-5096/$ - see front matter © 2003 Elsevier Ltd. All rights reserved.
doi:10.1016/j.jmps.2004.01.005

1. Introduction

The compressive failure of long fibre composites is of major concern for the design of composite structures since the compressive strength of practical laminates is significantly less than their tensile strength. Competing modes of compressive failure exist, including delamination, fibre failure and elastic and plastic microbuckling. A discussion of these different modes, and a map showing the regimes of dominance, has been constructed by Fleck (1997). A common failure mechanism for engineering composites is *imperfection-sensitive plastic microbuckling* from pre-existing fibre waviness. The phenomenon has received much attention in recent years, see for example, Budiansky and Fleck (1993), Moran et al. (1995), Kyriakides et al. (1995), Kyriakides and Ruff (1997), Hsu et al. (1998), Schapery (1995), Jensen and Christoffersen (1997), and Vogler et al. (2001); see also the reviews of Schultheisz and Waas (1996), Waas and Schultheisz (1996), and Fleck (1997).

While it is agreed that collapse is normally due to microbuckling, there is no consensus as to how the microbuckle is initiated. As compressive failure in composites is normally catastrophic, with little apparent damage before failure, it is difficult to determine from post-mortem examinations the precise sequence of events leading to failure. Hence models of microbuckle initiation have a valuable role to play. The thrust of much research has been to assume that regions of fibre waviness are the initiation sites, perhaps in co-operation with stress raisers such as free edges or resin rich regions (see for example Vogler and Kyriakides, 2001; Sutcliffe and Yuwono, 2001). This view has been challenged by several authors, who suggest an alternative initiation mechanism of fibre fracture leading to the onset of microbuckling (Lankford, 1995; Garland et al., 2001). While studies on model composites (Jelf and Fleck, 1992; Sutcliffe and Yuwono, 2001) show that fibre fracture is not required for microbuckle initiation, it remains a possible competing mechanism, with the actual failure mechanism for a particular composite system being the weakest one.

Previous microbuckling theory has concentrated on the prediction of failure from an idealised distribution of fibre misalignment, often in the form of an infinite band. In reality, composites possess random waviness, and there is a need to determine the relation between the distribution of compressive strength and the underlying statistical distribution of fibre waviness. The purpose of the current work is to obtain this relation for the case of a two-dimensional (2D) distribution of waviness.

1.1. Models of compressive failure with idealised fibre waviness

Argon (1972), observing that practical fibre composites have regions of fibre misalignment, considered kinking of an infinite band of inextensible fibres with a small initial fibre misalignment angle $\bar{\phi}$. For the case where the normal to the band is inclined at an angle $\beta = 0$ to the principal fibre direction, he derived a simple expression for the compressive strength σ_c of unnotched material as

$$\sigma_c = \frac{\tau_Y}{\bar{\phi}}, \tag{1}$$

where τ_Y is the shear yield stress of the rigid, ideally plastic composite. This infinite band model has been extended by Budiansky (1983) for the case of an elastic-perfectly plastic composite and by Budiansky and Fleck (1993) for a Ramberg–Osgood strain-hardening solid (detailed further in Section 2.1). They derived the compressive strength as

$$\sigma_c = \frac{G}{1 + n(\frac{3}{7})^{1/n}(\bar{\phi}/\gamma_Y/n - 1)^{(n-1)/n}}, \tag{2}$$

where G and γ_Y are the longitudinal shear modulus and shear yield strain of the composite, and n is the strain hardening exponent for Ramberg–Osgood power law hardening in shear.

The theories described above have an initial configuration in which there is an infinite band of misaligned fibres and an abrupt change of fibre orientation (a 'kink') at the boundaries of the band. Hence we here refer to these as 'kinking theories'. In practice, however, the bending stiffness of the fibres prevents such sharp kinks. To improve upon this, Fleck et al. (1995) proposed an infinite band analysis, including fibre bending, to estimate the compressive strength of fibre composites. They assumed that the fibres behave as linear elastic beams embedded within a non-linear dilatant matrix. The bending stiffness of individual fibres was homogenised by treating the composite as a Cosserat continuum capable of bearing couple stresses; the fibre diameter d acts as the pertinent length scale. Their results showed that inclusion of fibre bending increases the predicted compressive strength above kinking theory when the band width is less than about $30d$. Fleck and Shu (1995) generalised the one-dimensional (1D) analysis of Fleck et al. (1995) by treating the composite as a 2D Cosserat continuum with a bending resistance set by the fibre diameter d. Fleck and Shu (1995) embedded the 2D Cosserat continuum theory within a finite element (FE) code, and used this FE code to predict the compressive strength for an elliptical region of initial fibre misalignment under multi-axial loading (Fleck and Shu, 1995; Shu and Fleck, 1997). It was found that the dominant geometrical features are the magnitude of the initial fibre misalignment and the length ℓ of the elliptical region of waviness transverse to the overall fibre direction. The predicted collapse load approaches the infinite band predictions when ℓ exceeds about $200d$. More recently the theory has been used to investigate the reduction in compressive strength due to (i) the combined effects of waviness and macroscopic inhomogeneities such as holes and rigid inclusions (Fleck et al., 2000), and (ii) the presence of large-angle waviness under uniaxial compression and bending stress fields (Fleck and Liu, 2001). These studies provide a means of assessing how alternative defects, such as an array of fibre breaks, might initiate a microbuckle in the composite.

1.2. Random fibre waviness and the statistics of compressive strength

In practical composites the fibre misalignment angle varies throughout the composite in a random manner. In these circumstances it is not clear how to apply existing microbuckling models for well-defined waviness geometries (e.g. the infinite band models, Eqs. (1) and (2)). In particular, it is not obvious how to choose an appropriate value

for the fibre misalignment angle $\bar{\phi}$. As the compressive strength is sensitive to both the magnitude and wavelength of waviness, it is important to characterise the statistical nature of random fibre waviness with regard to both magnitude and wavelength.

Using 2D image analysis, Yurgatis (1987) and Jelf and Fleck (1992) measured the local fibre misalignment angle and showed that the misalignment angle is roughly Gaussian in nature; however, they did not give any information on the distribution of wavelength. Using an optical microscope, Kyriakides et al. (1995) examined the amplitude and wavelength of fibre misalignment along the overall fibre direction in APC-2/AS4 composites; they suggested that the wavelength is in the range of 300–800d with an amplitude in the range of 3–10d. Clarke et al. (1996) measured the 1D power spectral density of fibre slope in a glass fibre-reinforced epoxy by confocal laser-scanning microscopy. They observed that the wavelengths in the overall fibre direction are typically within the range of 70–600d; this range of wavelengths is in good agreement with that observed by Wisnom (1994) for carbon fibre composites. These studies and the work described in Section 2.4 provide the fibre waviness information required to assess whether fibre waviness is indeed sufficient to initiate microbuckling as commonly supposed.

Slaughter and Fleck (1994) have derived theoretical predictions for the statistical distribution of compressive strength for a 1D distribution of fibre waviness. The fibre misalignment angle was varied along the length of the fibre but was assumed to be invariant along a correlation direction inclined at an angle β to the transverse direction (thus, β is the initial orientation angle of the microbuckle band). This stochastic model of fibre waviness corresponds to the 'infinite band' model for idealised waviness as described by Argon (1972). The distribution of fibre waviness was given by a 1D spectral density function of fibre misalignment. They assumed a uniform power spectral density for fibre slope as a function of the distance s along the fibre direction, with an upper cut-off for the spectral frequency. Monte-Carlo realisations for fibre waviness were generated, and the compressive strength for each realisation was determined by the couple stress formulation of Fleck et al. (1995). The ensemble of results was then used to compute a probability density for compressive strength, and a Weibull fit was conducted to extract the Weibull parameters. Good agreement was observed between the predicted Weibull parameters and the values measured independently by Jelf and Fleck (1992).

1.3. Aims of the present study

In the current study, we aim to predict the distribution of compressive strength for unidirectional composites with an initial fibre waviness distributed in a random 2D manner. The unidirectional composite is treated as a 2D Cosserat continuum with a bending resistance set by the fibre diameter d. A stationary distribution of waviness is assumed, as characterised by a 2D power spectral density function. An ensemble of fibre waviness profiles is generated from the spectral density and the compressive strength for each individual fibre waviness profile is calculated using the finite element (FE) code of Fleck and Shu (1995). The relation between the dispersion in compressive strength and the details of the assumed spectral density function is explored. The spread

in strengths calculated from this direct FE approach is compared in Section 4 with that derived from an 'engineering' approach, based upon weakest link theory. The main novelty of the study is the analysis of 2D random waviness and the development of a 'fracture mechanics' type methodology to identity the worst flaw in the form of fibre waviness within the sample. The work addresses the issue as to whether a realistic level of fibre misalignment in long fibre composites can initiate microbuckling.

2. Theoretical model

The theoretical model is now outlined for the direct calculations of compressive strength. The constitutive law and FE implementation of Fleck and Shu (1995) are adopted. These are summarised in the following sections; details are given in Fleck and Shu (1995) and Shu and Fleck (1997). Section 2.4 describes the spectral density functions used to generate the random waviness profiles.

2.1. Constitutive law

The linear elastic fibres are assumed to carry couple stresses, whilst the matrix is assumed to deform in a non-linear manner under shear and transverse stress. A representative material element in the deformed configuration is shown in Fig. 1. The element is subjected to a longitudinal compressive stress component σ_L aligned with the fibre direction, a sliding shear stress τ_S, a transverse shear stress τ_T and a transverse tensile stress σ_T. The fibres endow the material element with a bending resistance, and the representative material element carries a bending moment per unit area, or couple stress, m. The fibres are modelled as Timoshenko beams and deform in bending and in shear. Thus, the cross-section of each fibre is assumed to rotate by an angle θ_f, which is, in general, different from the rotation of the neutral axis of the fibre ϕ. The initial misalignment angle is denoted by $\bar{\phi}$. A Lagrangian formulation is employed to describe the deformed configuration in terms of the initial reference configuration.

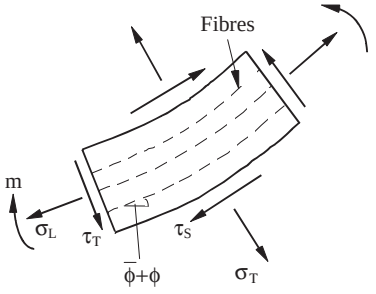

Fig. 1. Stress state for a representative material element of the fibre composite. The fibres rotate under load from an initial orientation $\bar{\phi}$ to a total rotation of $(\bar{\phi}+\phi)$.

The couple stress m within a representative material element is related to the fibre curvature $\kappa = \mathrm{d}\theta_\mathrm{f}/\mathrm{d}s$ by

$$m = \frac{E_\mathrm{L} d^2}{16}\kappa, \tag{3}$$

where s is the arc-length along the fibre in the deformed configuration, and E_L is the longitudinal modulus of the composite. Likewise, the longitudinal stress in the composite is given by the linear elastic relation

$$\sigma_\mathrm{L} = E_\mathrm{L} e_\mathrm{L}, \tag{4}$$

where e_L is the longitudinal elastic strain of the composite.

It is assumed that the composite deforms in a plane strain manner, and has a non-linear shear and transverse response, in accordance with a deformation theory version of plasticity (Shu and Fleck, 1997). As discussed by Shu and Fleck (1997), the particular choice of either a deformation or flow theory version of plasticity has a negligible effect upon the predicted compressive strength, but the deformation theory version of plasticity gives more accurate predictions for the combined transverse-shear strength under non-proportional loading, and is used herein. The main details of the deformation theory plasticity law of Shu and Fleck (1997) are summarised below. With axes aligned with the current fibre direction, the composite suffers a sliding shear strain γ_S and a transverse strain e_T associated with the sliding shear stress τ_S and transverse stress σ_T.

For the deformation theory version, an effective strain γ_e is defined in terms of γ_S and e_T:

$$\gamma_\mathrm{e} \equiv \sqrt{\gamma_\mathrm{S}^2 + R^2 e_\mathrm{T}^2}, \tag{5}$$

where R is taken as a material constant. Next, an effective shear stress τ_e is introduced as the work conjugate of γ_e, to give

$$\tau_\mathrm{e}\delta\gamma_\mathrm{e} = \tau_\mathrm{S}\delta\gamma_\mathrm{S} + \sigma_\mathrm{T}\delta e_\mathrm{T}. \tag{6}$$

On making use of Eqs. (5) and (6), τ_S and σ_T can be re-expressed as

$$\tau_\mathrm{S} = \tau_\mathrm{e}\frac{\partial\gamma_\mathrm{e}}{\partial\gamma_\mathrm{S}} = \tau_\mathrm{e}\frac{\gamma_\mathrm{S}}{\gamma_\mathrm{e}} \tag{7}$$

and

$$\sigma_\mathrm{T} = \tau_\mathrm{e}\frac{\partial\gamma_\mathrm{e}}{\partial e_\mathrm{T}} = R^2\tau_\mathrm{e}\frac{e_\mathrm{T}}{\gamma_\mathrm{e}}. \tag{8}$$

In the absence of fibre bending τ_T and γ_T become identical to τ_S and γ_S, respectively; in this limit the constitutive model is a simplified version of that presented by Sun and Chen (1989). These expressions can be inverted so that $(\gamma_\mathrm{S}, e_\mathrm{T})$ can be expressed in terms of $(\tau_\mathrm{S}, \sigma_\mathrm{T})$, and substitution into Eq. (5) provides an explicit expression for τ_e in terms of $(\tau_\mathrm{S}, \sigma_\mathrm{T})$,

$$\tau_\mathrm{e} \equiv \sqrt{\tau_\mathrm{S}^2 + \left(\frac{\sigma_\mathrm{T}}{R}\right)^2}. \tag{9}$$

Thus, R can be interpreted as the ratio of transverse yield strength to shear yield strength of the composite. (Typically, R is in the range of $R = 1$ to 2, as discussed by Fleck and Jelf, 1995.) The effective stress is related to the effective strain by the generalised Ramberg–Osgood law:

$$\frac{\gamma_e}{\gamma_Y} = \frac{\tau_e}{\tau_Y} + \frac{3}{7}\left(\frac{\tau_e}{\tau_Y}\right)^n, \tag{10}$$

where τ_Y is a shear yield strength, γ_Y is a shear yield strain and n is the strain hardening exponent. Under simple shear, γ_e reduces to γ, τ_e reduces to τ, and the initial slope of the shear stress–strain curve defines the shear modulus G with $G = \tau_Y/\gamma_Y$. Numerical values for the Ramberg–Osgood parameters (τ_Y, γ_Y, n) have been given for a range of composites by Jelf and Fleck (1994). The transverse yield strength of the composite σ_{TY} is given by $\sigma_{TY} \equiv R\tau_Y$, consistent with Eq. (5).

The composite is assumed to be plastically dilatant in transverse tension, as implied by relations (5), (9) and (10), while compressive transverse straining is treated as linear elastic, following the formulation of Shu and Fleck (1997). The details of the matrix response at the high tri-axial strains present in the microbuckle band are not clearly understood, but are thought to involve matrix yield, microcracking and rubble formation. Consequently the model is phenomenological in nature.

One limitation of the model is that it is 2D in nature. By calibrating the material response using measured data, 3D effects at a fibre level are implicitly included. The 2D plane strain model presented here cannot capture out-of-plane microbuckling commonly seen for thin laminates. Observations of the tip of propagating microbuckles show similar qualitative behaviour for in-plane and out-of-plane microbuckles (Sutcliffe and Fleck, 1994); nevertheless it would be interesting to explore further the influence of such 3D effects on microbuckle initiation.

2.2. Specification of composite properties

We use a single set of material properties appropriate to unidirectional carbon fibre reinforced epoxy. (The effect of material properties on compressive strength has been explored previously by Fleck and Shu, 1995.) The fibre volume fraction c is taken as uniform, with $c = 0.6$, and the ratio of transverse strength to shear strength is $R = \sqrt{2}$. Experimental data to obtain a precise value for R are limited, but the experiments of Fleck and Jelf (1995) suggest that this value is appropriate. An additional pragmatic assumption made in simplifying the constitutive relations is that R equals $\sqrt{E_T/G}$. The longitudinal elastic modulus E_L is taken to be 2000 times that of the shear yield strength τ_Y; the transverse modulus is $E_T = 200\tau_Y$, the shear modulus of the fibres is $G_f = 200\tau_Y$ and the shear modulus of the composite is $G = 100\tau_Y$.

The strain hardening index n for carbon fibre reinforced epoxy composites lies in the region of 3–10 (Jelf and Fleck, 1994). However, as shown by Fleck and Shu (1995), a variation in the strain hardening index n in the range of 3–10 has little effect upon the predicted compressive strength. In this paper the strain hardening index n is ascribed a value of 3.

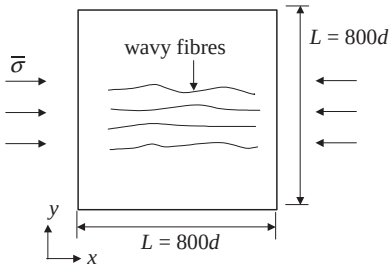

Fig. 2. Sketch of the finite element model.

2.3. Finite element implementation

The finite element implementation of Fleck and Shu (1995) is used. This procedure requires an expression for the global tangent stiffness matrix of the structure. The stiffness matrix is obtained from the rate form of virtual work for the governing field relations. For the constitutive model described above, Fleck and Shu (1995) derived the required rate form of virtual work from the following virtual work statement:

$$\int_V [\sigma_L \delta\varepsilon_L + \sigma_T \delta\varepsilon_T + \tau_S \delta\gamma_S + \tau_T \delta\gamma_T + m\delta\kappa]\, \mathrm{d}V = \int_S [t_i \delta u_i + q\delta\theta_f]\, \mathrm{d}S, \tag{11}$$

where the repeated lower-case suffix i denotes a sum from 1 to 2. The finite element implementation makes use of a Lagrangian formulation, and the rate problem includes any imbalance between the two sides of Eq. (11) associated with a drift from the equilibrium solution. The internal virtual work is calculated over the current volume V, and the external virtual work on the right-hand side is integrated over the current boundary S of the solid. The stress tractions t_i and the couple stress traction q are in equilibrium with the interior stress field and perform work through the displacement increments δu_i and the rotation increment $\delta\theta_f$, respectively. Eq. (11) is a statement of general Cosserat theory, and the rotation θ_f of the fibre cross-section is treated as an independent kinematic degree of freedom in addition to the two in-plane displacements u_i. This allows for the use of C_0-continuous elements in a finite element formulation. Here we omit the lengthy incremental form of the virtual work statement and refer the reader to Fleck and Shu (1995) for full details.

Six-noded triangular elements are employed, with 3 degrees of freedom at each node (two displacements and one rotation). The finite element procedure is based upon a Lagrangian formulation of the general finite deformation of the composite, and can deal with both geometrical and material non-linearities. A version of the modified Riks algorithm is adopted to handle the snap-back behaviour associated with the microbuckling response (Crisfield, 1991). An imperfection in the form of a spatial distribution of initial fibre misalignment $\bar{\phi}(x, y)$ is prescribed. Details of the assumed misalignment variation are described in Section 2.4.

Fig. 2 shows the square model geometry, of side length $L = 800d$, used for all the calculations of strength with random waviness. Each finite element is of side length

$8d$ (giving 100 elements along each side of the model). The x-axis is aligned with the nominal fibre direction and the y direction is transverse to the fibres. The uniaxial compressive stress $\bar{\sigma}$ applied along the fibre direction specifies the average axial traction t_x over the end face, with zero shear and transverse loading. Periodic boundary conditions are imposed along all four edges of the mesh, and the equilibrium path of $\bar{\sigma}$ versus mean shortening of the periodic unit cell is calculated by the Riks algorithm. The method follows that described by Chen et al. (1999).

2.4. Distribution of initial fibre misalignment

In unidirectional engineering composites, fibre misalignment is stochastic in nature. Assuming that the fibre misalignment distribution is statistically independent of position, i.e. that it is a stationary random function, conventional signal processing theory can be used to model the waviness (Newland, 1984). The distribution of fibre misalignment can be characterised by the spectral density of fibre slope $\alpha = \tan\bar{\phi}$, and this function describes how different frequencies (or wavelengths) contribute to the total mean square amplitude of the signal.

In this study, we adopt the strategy of Slaughter and Fleck (1994), who assumed simplified forms of spectral density function based on the 1D spectral density measurements of Clarke et al. (1996). Recently, Creighton et al. (2001) have developed an accurate and semi-automated image analysis procedure to measure in-plane 2D fibre misalignment distributions in unidirectional fibre composites. This method has been used by the present authors to measure waviness distributions for the same carbon fibre epoxy composite laminates as examined by Creighton et al. (2001). Fig. 3 shows the single-sided spectra, along and transverse to the fibre direction, for three samples (two at low magnification to measure the low-frequency signal, and one at higher magnification for the high-frequency part of the spectrum). The upper abscissa axis gives the corresponding wavelength scale, normalised by the fibre diameter d of 6 μm. The results confirm the observations of Clarke et al. (1996) and Wisnom (1994), that the main contribution to the waviness comes from wavelengths on the order of a few hundred d. Perhaps unexpectedly, given the anisotropic nature of the material and processing route, there is no significant difference between the spectra in the axial and transverse directions. Although only a preliminary study, the results of Fig. 3 suggest that the square and exponential functions used by Slaughter and Fleck (1994) for their 1D analysis are reasonable idealisations of the spectral density for a 2D analysis, with the same dependence of spectral density upon frequency in both the axial and transverse directions. Hence the current study uses the following two forms of 2D spectral density for fibre slope $S(\omega_x, \omega_y)$, as a function of the spatial frequencies ω_x and ω_y in the fibre direction and transverse to the fibres, respectively:

(i) Square wave function:

$$S(\omega_x, \omega_y) = \begin{cases} S_0 & \text{if } |\omega_x| \leqslant \omega_c \text{ and } |\omega_y| \leqslant \omega_c, \\ 0 & \text{if } |\omega_x| > \omega_c \text{ or } |\omega_y| > \omega_c. \end{cases} \tag{12}$$

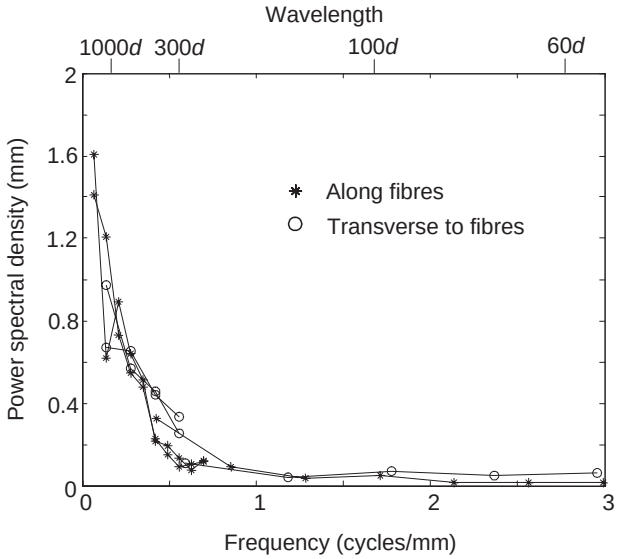

Fig. 3. Measured single-sided power spectral density functions along the fibre direction, and in the transverse direction for carbon fibre epoxy composite specimens. The upper abscissa gives a wavelength scale normalised by the fibre diameter $d = 6$ μm.

(ii) Exponential function:

$$S(\omega_x, \omega_y) = S_0 \mathrm{e}^{-((\omega_x/\omega_c)^2+(\omega_y/\omega_c)^2)}, \tag{13}$$

where ω_c is a 'cut-off' wavelength, assumed equal in the x and y directions. Cross sections of the two spectral density functions along the line $\omega_y = 0$ are illustrated in Fig. 4. The amplitude of the waviness is characterised in Eqs. (12) and (13) by the spectral parameter S_0. The mean square amplitude Σ^2 of the fibre slope is used to compare the two spectral functions, using the property that Σ^2 is equal to the area under the spectral density function. A typical value of $\Sigma^2 = 1.5 \times 10^{-4}$ is used, except where stated, corresponding to a r.m.s. misalignment angle of 0.7°. This value of Σ^2 is close to that of the samples whose spectra are given in Fig. 3. Since the nominal fibre direction is taken to lay along the x-axis, the amplitude of the fibre slope for infinite wavelength (zero frequency) in the x direction is put equal to zero (i.e. $S(0,0) = 0$). The minimum frequency that can be represented is limited by the side length L of the periodic mesh, and equals $2\pi/L = 0.008/d$; the smooth spectra, as described by Eqs. (12) and (13), are represented by a discrete series of points with spacing equal to this minimum frequency, as sketched schematically in Fig. 4. Typically, a value of $\omega_c = 0.08/d$ is used, so that the discrete representation of the smooth spectra as defined by Eqs. (12) or (13) is adequate. Values of ω_c between $0.02/d$ and $0.08/d$ are used, corresponding to cut-off wavelengths of between about $300d$ and $80d$, respectively. These values are consistent with the values seen in Fig. 3 and observed by Wisnom

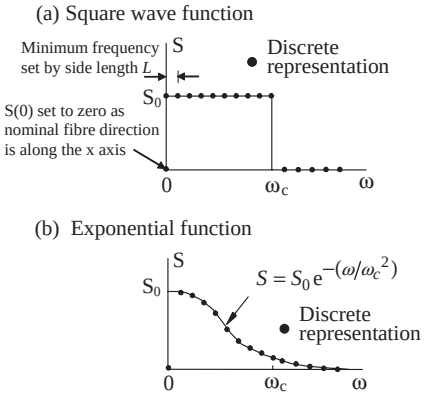

Fig. 4. A section through the plane $\omega_y = 0$ for two shapes of spectral density: (a) square wave function and (b) exponential function. The dots show the discrete representations of the smooth forms given by the corresponding Eqs. (12) and (13).

(1994) and Clarke et al. (1996). The nodal spacing of $4d$ allows frequencies up to the maximum cut-off used of $\omega_c = 0.08/d$ to be represented accurately.

2.5. Calculation method

The Monte Carlo method is used to obtain the statistical distribution of compressive strength. For a given spectral density, individual realisations of fibre misalignment profile (in the form of fibre slope α) are created using the fast Fourier transform (FFT) method (Cebon and Newland, 1984). Each realisation has zero mean fibre slope and the desired spectral density; a detailed description of the method by which the realisations are constructed is given in Appendix A. The collapse strength for each realisation is calculated and probability curves of collapse strength are obtained. Thus, the relationship between the spectral density and the distribution of collapse strength is obtained.

3. Results of FE calculations of strength for random waviness

In this section, the compressive strengths of an ensemble of waviness profiles generated from a given spectral density are calculated by the finite element method described above. The effect of the initial waviness distribution is explored, and results are interpreted in terms of Weibull statistics. An engineering approach to reproduce these results is described in Section 4.

3.1. Collapse response

A typical plot of the average axial stress $\bar{\sigma}$ versus end shortening $\bar{u}_x$ is given in Fig. 5, for a typical waviness profile generated from the square wave spectral density function with $\omega_c = 0.08/d$ and $\Sigma^2 = 1.5 \times 10^{-4}$. The overall response shown in Fig. 5

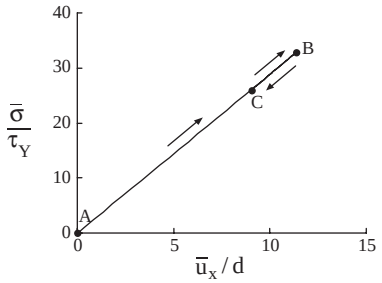

Fig. 5. Load versus end shortening displacement curve for a typical fibre waviness profile ($\omega_c = 0.08/d$, $\Sigma^2 = 1.5 \times 10^{-4}$).

is very nearly linear up to the peak load $\bar{\sigma}_c$, at which point sharp snap-back behaviour is observed. A similar unstable response is seen experimentally (see for example Kyriakides et al., 1995); in addition there is typically a slight reduction in slope during loading associated with a reduction in fibre modulus, followed by catastrophic failure. Since we focus our attention on the initiation and early propagation of a microbuckle, the calculation of post-buckling response was terminated when the load dropped to about 80% of the peak value. The progressive nature of collapse is exhibited by the contours of total fibre rotation $\phi_t = \bar{\phi} + \phi$ shown in Figs. 6a–c for the states A–C as labelled in Fig. 5. State A is the initial unloaded configuration with $\phi_t = \bar{\phi}$; state B is at maximum load and the post-buckled state C is at 80% of maximum load. Fig. 6 reveals that collapse involves the initiation and growth of a microbuckle from a large damaging patch of fibre misalignment. Fleck (1997) describes calculations which track the further evolution of the microbuckle, showing how a microbuckle evolves from the initiation site.

3.2. Probability distribution of compressive strength

The cumulative probability distribution of strength $P(\bar{\sigma}_c/\tau_Y)$ is computed from a large number of realisations (typically 45), all with the same assumed spectral density of fibre misalignment. Fig. 7 shows the sensitivity of strength distribution to the mean square amplitude Σ^2, for the square wave spectral density function with $\omega_c = 0.08/d$ and Σ^2 in the range 0.5×10^{-4}–2×10^{-4}. The figure includes results for the exponential spectral density function with $\omega_c = 0.08/d$ and $\Sigma^2 = 1.5 \times 10^{-4}$. The cumulative functions express the probability of survival as a function of the applied load $\bar{\sigma}_c/\tau_Y$. At a sufficiently low load all the realisations survive. The proportion of the samples that fail rises as the applied stress increases, and the probability of failure reaches 1 at a sufficiently high stress. Fig. 7 shows that the difference between the cumulative probability distributions for the square and exponential spectral density functions is small and hereafter we consider only the square shape of spectral density. The effect of increasing the mean square amplitude Σ^2 of the fibre slope is to shift the probability distributions to lower values of compressive strength. This conclusion mirrors results for 1D microbuckling theory (cf. Eq. (1)); the higher is the fibre misalignment the lower is the compressive

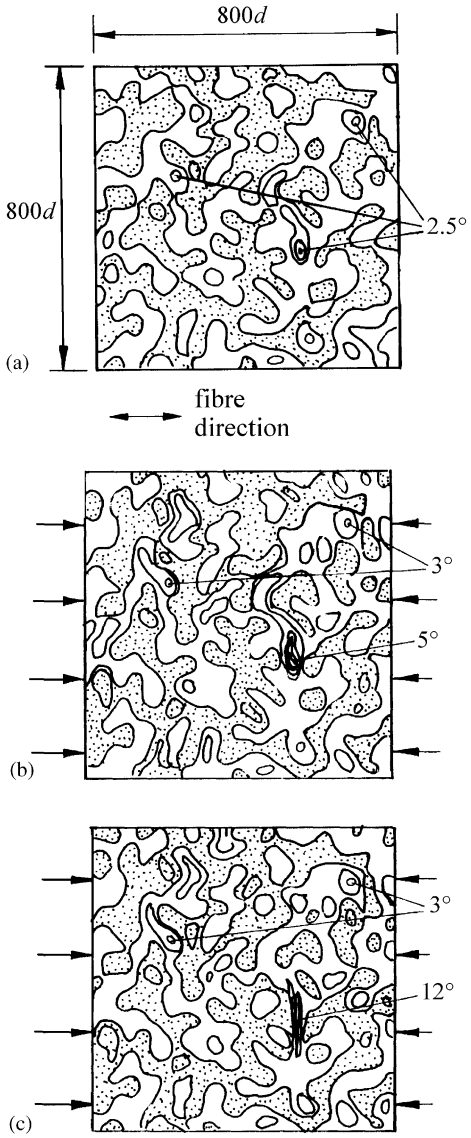

Fig. 6. Contours of fibre misalignment $(\bar{\phi}+\phi)$ corresponding to the load–displacement curve of Fig. 5 with $\omega_c = 0.08/d$, $\Sigma^2 = 1.5\times10^{-4}$. Contours are drawn at $(\bar{\phi}+\phi) = -1°$, 0° and 1°, except where indicated, with regions of negative $(\bar{\phi}+\phi)$ shaded: (a) initial fibre waviness, state A, (b) total fibre rotation $\phi_t \equiv \bar{\phi}+\phi$ at peak load, state B and (c) total fibre rotation at 80% of peak load, state C.

strength. The results of Fig. 7 for the square wave spectral function are replotted in Fig. 8 to show contours of survival probability P as a function of mean square misalignment angle Σ^2 and applied stress $\bar{\sigma}_c/\tau_Y$. This shows the usual behaviour: an increase in waviness leads to a reduction in strength.

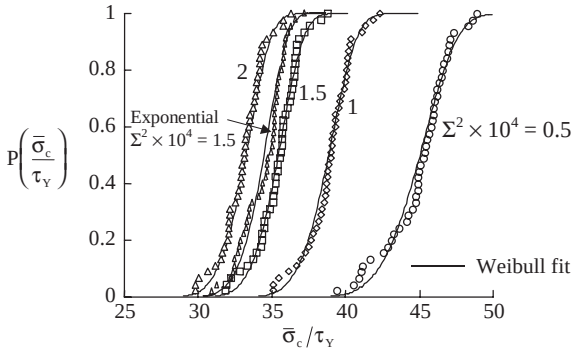

Fig. 7. Effect of mean square fibre misalignment amplitude Σ^2 and spectrum shape on the cumulative probability function for compressive strength $P(\bar{\sigma}_c/\tau_Y)$, with $\omega_c = 0.08/d$. Results are shown for the square wave spectral density function (13), except where indicated. The lines are curve fits using the Weibull model.

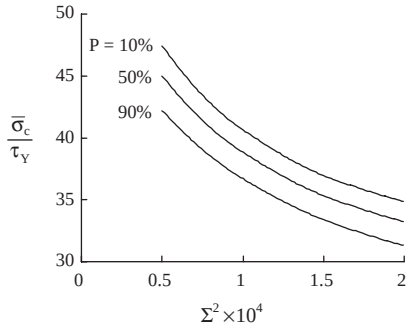

Fig. 8. Contours of constant probability of survival P as a function of mean-square misalignment angle Σ^2 and applied stress $\bar{\sigma}_c/\tau_Y$ for the square wave spectral function with $\omega_c = 0.08/d$.

The effect of cut-off frequency ω_c on the cumulative probability function for compressive strength is shown in Fig. 9, for the square wave spectral density function with $\Sigma^2 = 1.5 \times 10^{-4}$. Fig. 9 shows that the strength increases with increasing cut-off frequency ω_c, with the following explanation. Although the mean square fibre slope Σ^2 remains fixed, the relative contribution from short wavelengths (high frequencies) increases with increasing cut-off frequency. Since these short wavelength imperfections give rise to higher microbuckling strengths, associated with the bending resistance of the fibres, the strength of the composite tends to increase. The same reasoning explains the slightly higher strengths seen in Fig. 7 for the square spectral density function, as compared with the exponential function, on account of the lower proportion of long wavelengths (short frequencies) for the square wave function.

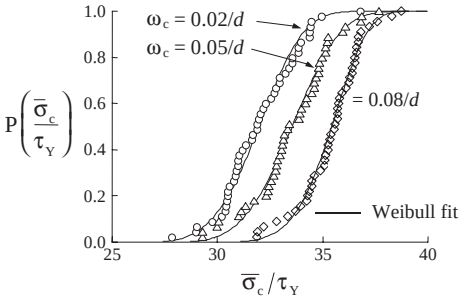

Fig. 9. Effect of cut-off frequency ω_c on the cumulative probability function $P(\bar{\sigma}_c/\tau_Y)$ for the compressive strength due to the square wave spectral density function, $\Sigma^2 = 1.5 \times 10^{-4}$.

3.3. Weibull model of compressive strength and comparison with experimental data

The Weibull model of failure for brittle solids supposes that cracking occurs from the largest flaw. Since the results described above show that compressive failure in fibre composites is due to microbuckling failure from the largest imperfection, it is appropriate to attempt to curve fit the Weibull model to the present results. Fig. 7 shows that the probability curve for the square wave spectrum with parameters $\omega_c = 0.08/d$ and $\Sigma^2 = 1.5 \times 10^{-4}$ are well matched by the Weibull curve

$$P\left(\frac{\bar{\sigma}_c}{\tau_Y}\right) = 1 - \exp\left[-\left(\frac{\bar{\sigma}_c/\tau_Y - \bar{\sigma}_u}{\bar{\sigma}_0}\right)^m\right] \tag{14}$$

with fitting parameters $\bar{\sigma}_u$=28.6, $\bar{\sigma}_0$=7.25 and m=5.60, determined by the least-squares method. Similar fits are obtained for other spectral density parameters. Slaughter and Fleck (1994) have determined the Weibull parameters $\bar{\sigma}_0$ and m based on a 1D spectral density in the form of a square wave. They found $\bar{\sigma}_0 = 7.54$ and $m = 5.41$, which are in very good agreement with those found here. The value for the Weibull modulus $m = 5.60$ is also in reasonably good agreement with the value of $m = 6.1$ determined experimentally by Jelf and Fleck (1992) for carbon fibre reinforced PEEK. It is conjectured that Weibull theory can also be applied to model the effect of specimen size upon strength, and the resolution of this issue awaits a future study. The relatively low value of Weibull modulus emphasises the importance of the statistical modelling to derive accurate estimates of strength for fibre composites in compression. The mean predicted strength shown in Fig. 9 of between $32\tau_Y$ and $35\tau_Y$, depending on the cut-off wavelength, is close to the mean strength measured by Jelf and Fleck (1992) of the order of $28\tau_Y$. The good correlation between the measurements and the predictions using a practical distribution of fibre waviness strongly supports the hypothesis that microbuckle initiation can be attributed to fibre waviness in engineering composites. Of course other mechanisms such as fibre failure or delamination may come into play where these modes are particularly weak in a given composite system.

4. An 'engineering model' to predict compressive strength

Sections 2 and 3 show how the compressive strength of a fibre composite with random fibre waviness can be predicted using an appropriate Cosserat model for composites, with the distribution in strength fitted by the Weibull model. In this section we show how the results of this time-consuming calculation can be reproduced approximately using a much simpler engineering approach, based upon fracture mechanics principles.

In a specimen with random fibre waviness, a microbuckle initiates from the most damaging patch of fibre misalignment. The question arises: can the compressive strength due to this most damaging wavy patch be predicted from a knowledge of the strength for idealised fibre misalignments? For the case of idealised patches of fibre misalignment, such as the circular or elliptical patches described below, the size and amplitude of the misaligned region can be identified straightforwardly. However, for random waviness such as that shown in Fig. 6a it is not obvious how to extract an effective patch size and amplitude. The solution adopted herein is to apply a line 'filter' to the random waviness profile to search for the patch of waviness with the most damaging combination of physical size and misalignment angle. Because the width of the misaligned patch (transverse to the mean fibre direction) is the critical geometric parameter, line scans along the transverse y-direction of the specimen are considered. These are spaced a distance $8d$ apart in the longitudinal x direction, so that the scanned area is comprehensively covered. The locations of zero fibre misalignment along each scan demark the boundaries between adjacent patches of waviness. This allows the line scan to be split up into individual segments of fibre misalignment, each with a corresponding length ℓ and line-average waviness amplitude $\bar{\phi}_{\mathrm{av}}$ (i.e. taking the average fibre misalignment angle along the line segment between adjacent locations of zero misalignment). A number of alternative schemes have been tried, for example considering the mean waviness amplitude over an area, rather than along a line, but the simple line-average approach proved to be the most robust and effective.

For each wavy patch identified in the random structure, we need to predict the associated compressive strength; the overall strength of the composite will be given by the weakest patch in the specimen. The idealised circular and elliptical geometries shown in Fig. 10 are used to construct a look-up table giving the dependence of strength upon imperfection size and amplitude. For both geometries, the length of the patch transverse to the fibre direction is ℓ. For the elliptical patch the length along the fibre direction is held fixed at $20d$ and the major axis of the ellipse is aligned with the fibre direction. Calculations showed that rotation of the axis of the ellipse by 30° makes a relatively small change in the predicted strength. For both waviness geometries the fibre misalignment varies in the following cosine manner, falling to zero at the edge of the patch;

$$\bar{\phi} = \begin{cases} \bar{\phi}_0 \cos\dfrac{\pi}{2}\rho & (\rho \leqslant 1), \\ 0 & (\rho > 1). \end{cases} \tag{15}$$

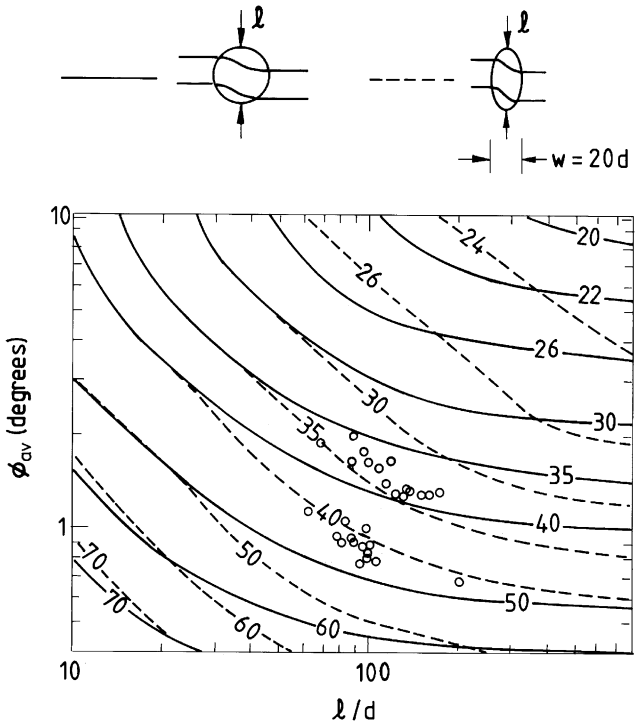

Fig. 10. Contours of compressive strength $\bar{\sigma}_c/\tau_Y$ for a circular wavy patch and for an elliptical wavy patch ($w = 20d$) as a function of length ℓ and line-average misalignment angle $\bar{\phi}_{av}$. Solid lines—circular patch; dashed lines—elliptical patch. The circular symbols show the length and average fibre misalignment angle of the critical patch of waviness for each realisation of random waviness using the square wave spectral function with $\omega_c = 0.08/d$. The top cluster of points are for $\Sigma^2 = 1.5 \times 10^{-4}$ (corresponding to $\Sigma = 0.7°$), while the bottom group are for $\Sigma^2 = 0.5 \times 10^{-4}$ ($\Sigma = 0.4°$).

For the circular patch, ρ equals $2r/\ell$ where r is the radius from the centre of the imperfection, while for the elliptical patch of length 2ℓ and width $2w$ we have

$$\rho = \left\{ \left(\frac{2x_1}{w} \right)^2 + \left(\frac{2y_1}{\ell} \right)^2 \right\}^{1/2} . \tag{16}$$

The local co-ordinate (x_1, y_1) has its origin located at the centre of the imperfection with axis x_1 parallel to the global fibre direction. The maximum fibre misalignment angle $\bar{\phi}_0$ is related to the line-average fibre misalignment $\bar{\phi}_{av}$ through the centre of the patch by $\bar{\phi}_{av} = 2\bar{\phi}_0/\pi$. The calculation of the strength follows the procedure given in Section 2, with the size of the domain containing the wavy patch chosen to be much larger than the size of the patches. Fig. 10 plots contours of maximum strength for the two geometries as a function of patch size and mean fibre misalignment, while these results are tabulated in Tables 1 and 2 for the circular and elliptical geometries, respectively. The maximum strength is seen at the bottom left of the figure with the

Table 1
Compressive strength $\bar{\sigma}_c/\tau_Y$ for a circular patch of waviness as a function of diameter ℓ and line-average misalignment $\bar{\phi}_{av}$

$\bar{\phi}_{av}$ (°)	$\ell = 10d$	$\ell = 15d$	$\ell = 20d$	$\ell = 30d$	$\ell = 40d$	$\ell = 80d$	$\ell = 100d$	$\ell = 200d$	$\ell = 400d$	$\ell = 800d$
0.40	80.32	75.30	72.36	69.16	67.13	63.94	63.15	61.61	60.74	60.32
0.64	73.02	68.03	64.86	60.50	58.00	53.00	51.70	48.60	47.50	46.74
0.80	69.84	63.91	60.83	56.20	53.90	49.13	47.82	44.96	43.93	43.15
0.96	66.67	60.70	57.10	52.95	50.60	46.00	44.80	42.40	41.38	40.72
1.28	62.60	56.87	53.30	49.10	46.40	41.83	40.67	38.17	36.98	36.23
1.90	56.48	50.90	47.55	43.50	41.00	36.63	35.61	33.20	32.30	31.78
2.55	52.31	46.70	43.57	39.45	36.99	32.86	31.60	29.40	28.50	28.05
3.82	47.10	41.68	38.67	35.30	33.29	29.45	28.50	26.64	25.89	25.47
5.10	44.02	38.76	35.77	32.54	30.57	26.80	25.80	23.85	22.96	22.59
7.64	40.58	35.72	32.93	29.85	27.80	24.12	23.16	21.50	20.60	20.26
10.20	38.87	34.32	31.70	28.84	26.76	23.01	22.20	20.68	19.87	19.58

Table 2
Compressive strength $\bar{\sigma}_c/\tau_Y$ for an elliptical patch of waviness of width $20d$ as a function of length ℓ and line-average misalignment $\bar{\phi}_{av}$

$\bar{\phi}_{av}$ (°)	$\ell = 10d$	$\ell = 15d$	$\ell = 20d$	$\ell = 30d$	$\ell = 40d$	$\ell = 80d$	$\ell = 100d$	$\ell = 200d$	$\ell = 400d$	$\ell = 800d$
0.40	84.35	76.36	72.36	67.24	63.36	56.24	55.03	51.10	48.68	47.13
0.64	77.32	69.53	64.86	58.20	54.20	46.95	45.50	42.30	40.10	38.81
0.96	68.97	62.10	57.29	51.46	47.80	40.94	39.53	36.18	33.92	32.83
1.28	64.34	58.10	53.60	47.85	44.54	37.45	35.95	32.45	30.20	29.23
2.00	56.85	50.72	46.82	42.13	39.30	33.47	32.01	28.50	26.40	25.56
2.55	52.51	47.20	43.77	39.45	36.73	31.55	30.31	27.30	25.50	24.73
3.82	47.10	41.68	38.67	35.30	33.29	29.45	28.50	26.23	24.62	23.92
5.10	44.02	38.76	35.77	32.34	30.75	27.75	26.99	25.45	24.12	23.63
7.64	40.58	35.72	32.80	29.95	28.28	25.99	25.36	24.40	23.45	23.04
10.00	38.85	34.32	31.76	28.95	27.32	25.30	24.89	23.82	23.10	22.80

smallest misalignment angle and smallest patch size. For typical misalignment angles on the order of 2° the strength increases significantly for patches smaller than about $100d$ due to the effect of fibre bending stiffness. Sample calculations for the circular patch revealed that the compressive strength for a cosine distribution of fibre misalignment is close to those for alternative square- or triangular-wave spatial distributions of fibre misalignment, with a fixed value of average fibre misalignment $\bar{\phi}_{av}$; this justifies the use of the line-average misalignment to characterise the fibre waviness in a patch.

In summary, the procedure described below is used to predict the compressive strength due to random waviness:

1. Apply the line-filter to the random waviness geometry to identify a set of waviness patch lengths ℓ and corresponding fibre misalignment angles $\bar{\phi}_{av}$.

2. Estimate the compressive strength for each of the patches thus identified, using the results of Tables 1 or 2 for circular or elliptical patches of waviness with the same values of ℓ and $\bar{\phi}_{av}$. Linear interpolation is used between tabulated data. The strength of the weakest patch is taken as the overall compressive strength for the specimen.

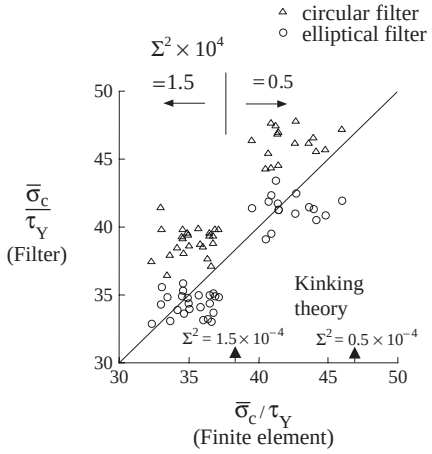

Fig. 11. Comparison between direct finite element calculations and the predictions using the engineering filter model with either the circular or elliptical look-up tables, for the compressive strength of a group of fibre waviness profiles generated using the square spectral profile ($\omega_c = 0.08/d$). Predictions using kinking theory, Eq. (2), with the effective fibre waviness equal to Σ, are shown by arrows on the abscissa.

The accuracy of the above filter procedure is assessed in Fig. 11, for arbitrarily selected waviness profiles generated from a square wave spectral density function with $\omega_c = 0.08/d$ and $\Sigma^2 = 0.5$ and 1.5×10^{-4}. Fig. 11 shows that the predictions based on a circular wavy patch over-estimate the compressive strength by a factor of about 20% in comparison with the finite element results. The predictions for compressive strength based on an elliptical wavy patch are in excellent agreement with the finite element results. The geometry of the critical patch for each realisation, based on the elliptical patch strength, is included in Fig. 10, illustrating the dispersion in size and fibre misalignment angle generated by the random nature of the waviness. Fig. 10 shows that the critical patch length ℓ is around $100d$. The line-average misalignment angle of the critical patch is a factor of between 2 and 3 times greater than the corresponding r.m.s. misalignment angle Σ.

One may wonder why calculations using an elliptical wavy patch offer better predictions for strength with random waviness than those with the circular patch. The following explanation is offered.

1. The statistical nature of the generated waviness ensures that patches of waviness are not in general circular, even for a waviness profile associated with an isotropic spectral density function. Elliptical patches which are elongated along the transverse direction are weaker than patches of the same shape and size orientated along the fibre direction. Hence the critical patch in a random fibre waviness distribution is statistically more likely to be elongated in the transverse direction.

2. Tables 1 and 2 do not consider the effect of interaction between neighbouring patches of fibre misalignment. This effect is explored in Fig. 12, showing the knock-down factor in strength associated with interaction between two circular patches of misalignment separated by a distance S. Calculations are performed for two patch diameters

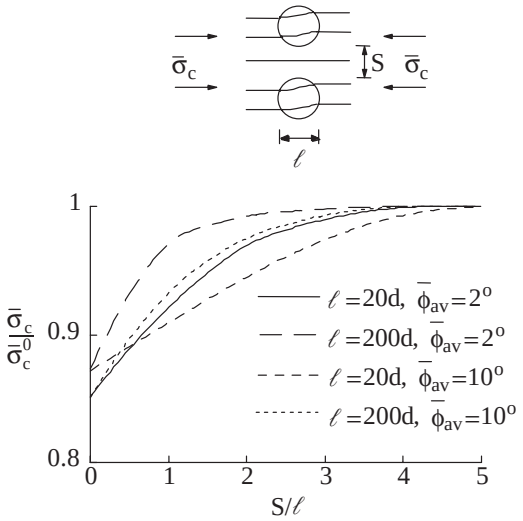

Fig. 12. Knockdown in compressive strength $\bar{\sigma}_c$ due to the interaction between two identical circular wavy patches aligned in the transverse y-direction and separated by a distance S, relative to the strength $\bar{\sigma}_c^0$ for a single circular patch of waviness.

and for two mean misalignment angles, as detailed in the figure, and compared with the corresponding strength for a single circular patch. Fig. 12 shows that there is a slight reduction in the compressive strength due to the interaction between adjacent wavy patches. Thus the calculations based on a circular wavy patch offer upper bound estimates for compressive strength for a specimen containing many wavy patches.

5. Kinking theory applied to random waviness

Kinking theory provides a simple way of predicting the compressive strength of composites with random waviness; here we adopt the r.m.s. fibre misalignment angle Σ as an estimate of the misalignment angle $\bar{\phi}$. The corresponding predictions of kinking theory, Eq. (2), are indicated by arrows on the abscissa of Fig. 11, showing that this approach gives a reasonable first order estimate for the strength. However this reasonable agreement relies upon two competing factors:

(i) kinking theory neglects the fibre bending resistance and thereby underestimates the strength;

(ii) the use of Σ as the misalignment angle leads to an underestimate of the critical misalignment angle present in the specimen, cf. Fig. 10.

6. Concluding remarks

A finite element model for fibre composites, including the role of fibre bending resistance, has been used to investigate the compressive strength of composites con-

taining a 2D random distribution of fibre misalignment. The fibre misalignment angle is characterised by a power spectral density function, describing the contributions of different wavelengths to the overall fibre misalignment distribution. The spectral density function used is based on experimental measurements of a long fibre carbon epoxy composite. The distribution of strengths is evaluated using the Monte Carlo method: a large number of realisations for fibre waviness distribution are constructed for a given spectrum of waviness, and the strength distribution is constructed by calculating the strength of each realisation.

The sensitivity of compressive strength to the spectral parameters has been investigated. The strength of the composite decreases with increasing mean fibre misalignment angle. For the same mean misalignment angle, an increase in the cut-off frequency above which no components of waviness are present leads to a drop in strength. This is because the overall proportion of short wavelength components rises with increasing cut-off frequency. The short wavelength components are less damaging than long wavelength components due to the greater contribution of fibre bending stiffness to strength. Details of the shape of the spectrum (from an exponential to a square wave function) have only a minor influence upon the strength distribution. The probability distribution of compressive strength is well matched by a Weibull fit. In particular, the magnitude of the Weibull modulus is in agreement with that measured experimentally by Jelf and Fleck (1992). The predicted strength based on realistic fibre misalignment distributions is comparable to that observed for carbon fibre epoxy composites, confirming the hypothesis that fibre waviness can initiation microbuckling.

An engineering model is proposed to predict compressive strength for a random distribution of waviness by identifying the most damaging patch of fibre misalignment. A line-filter is applied to the random waviness to identify the size and average misalignment angle of the waviness patches in the specimen. The strength due to each patch of imperfection is estimated via a look-up table derived for circular and elliptical patches of waviness. The prediction based on an elliptical wavy patch gives excellent predictions for strength while the prediction based on a circular patch over-estimates the compressive strength by a factor of about 20%. Kinking theory based on the r.m.s. fibre misalignment gives a reasonable first approximation to the strength but is unable to capture the statistical distribution of strength.

As well as giving insight into the mechanism of microbuckle initiation and hence the factors governing compressive strength, this study contributes to understanding the origin of scatter in compression strength data. The approach provides a sensitivity analysis of the statistics of macroscopic strength to the micromechanical details. Hence this provides a formalism for interpreting experimental data and guiding developments to improve the compressive strength of composites, for example by changes in material properties, laminate design or processing route.

Appendix A. Generation of random fibre waviness distributions

In this appendix we review the signal processing theory used to generate 2D random fibre waviness distributions from a given spectral density function, following the

methods described by Newland (1984) and Cebon and Newland (1984). Consider a 2D distribution (of fibre misalignment) $f(x,y)$, sampled discretely over the intervals $x=(0,L_x)$ and $y=(0,L_y)$. Let $f_{k,m}=f(x_k,y_m)$ where $x_k=k\Delta_x$ and $y_m=m\Delta_y$, $k=0,1,\ldots,N_x-1$, $m=0,1,\ldots,N_y-1$, $\Delta_x=L_x/N_x$ and $\Delta_y=L_y/N_y$. The discrete Fourier transform $F_{k,m}$ of $f_{k,m}$ is

$$F_{k,m}=\frac{1}{N_xN_y}\sum_{r=0}^{N_x-1}\sum_{s=0}^{N_y-1}f_{r,s}\exp\left(-2\pi\mathrm{i}\left(\frac{kr}{N_x}+\frac{ms}{N_y}\right)\right)\quad\begin{cases}k=0,1,\ldots,N_x-1,\\ m=0,1,\ldots,N_y-1.\end{cases}\tag{A.1}$$

If ω_{x0} and ω_{y0} are the maximum frequency components present in $f(x,y)$ in the x and y directions respectively, then it is required that $N_x>\omega_{x0}L_x/\pi$ and $N_y>\omega_{y0}L_y/\pi$ in order to avoid aliasing (an accuracy eroding artifact of the implicit assumption that the sampled distribution is periodic). Important properties of $F_{k,m}$ are

$$F_{-k,-m}=F^*_{k,m},\quad F_{k,N_y-m}=F_{k,-m},\quad F_{N_x+k,m,N_y+m}=F_{k,m},\tag{A.2}$$

where F^* denotes the complex conjugate of F. Consequently

$$|F_{-k,-m}|=|F_{k,m}|,\quad |F_{k,N_y-m}|=|F_{k,-m}|,\quad |F_{N_x-k,N_y-m}|=|F_{k,m}|.\tag{A.3}$$

$\hat{S}(\omega_x,\omega_y)$, the linear spectral density of $f(x,y)$, is defined as the Fourier transform of its autocorrelation function. We sample $\hat{S}(\omega_x,\omega_y)$ discretely over the intervals $x=(0,L_x)$ and $y=(0,L_y)$ and we define $\hat{S}_{k,m}\equiv\hat{S}(\omega_{xk},\omega_{ym})$, where $\omega_{xk}\equiv 2\pi k/L_x$, $\omega_{ym}\equiv 2\pi m/L_y$, $k=0,1,\ldots,N_x-1$ and $m=0,1,\ldots,N_y-1$. The discrete *linear* spectral density is related to the DFT $F_{k,m}$ by

$$\hat{S}_{k,m}\cong\frac{L_xL_y}{(2\pi)^2}F^*_{k,m}F_{k,m}=\frac{L_xL_y}{(2\pi)^2}|F_{k,m}|^2.\tag{A.4}$$

It follows from Eq. (A.3) that

$$\hat{S}_{-k,-m}=\hat{S}_{k,m},\quad \hat{S}_{k,N_y-m}=\hat{S}_{k,-m},\quad \hat{S}_{N_x-k,m,N_y-m}=\hat{S}_{k,m}.\tag{A.5}$$

Given a spectral density function $\hat{S}(\omega_x,\omega_y)$, the following procedure is used to generate random realisations of the discrete distribution $f_{k,m}=f(kL_x/N_x,mL_y/N_y)$ of increments $\Delta_x=L_x/N_x$ and $\Delta_y=L_y/N_y$:

(1) Identify cut-off frequencies ω_{x0} and ω_{y0} above which $\hat{S}(\omega_x,\omega_y)$ is zero (or approximately zero). Choose even integers N_x and N_y appropriate for the desired refinement and satisfying $N_x>\omega_{x0}L_x/\pi$ and $N_y>\omega_{y0}L_y/\pi$.

(2) Sample the spectral density and enforce the constraint (A.5) to obtain

$$\hat{S}_{k,0}=\hat{S}\left(\frac{2\pi k}{N_x\Delta_x},0\right),\quad k=0,1,2,\ldots,N_x/2,$$

$$\hat{S}_{N_x-k,0}=\hat{S}_{k,0},\quad k=N_x/2+1,\ldots,N_x-1,$$

$$\hat{S}_{0,m}=\hat{S}\left(0,\frac{2\pi m}{N_y\Delta_y}\right),\quad m=1,2,\ldots,N_y/2,$$

$$\hat{S}_{0,N_y-m} = \hat{S}_{0,m}, \quad m = N_y/2+1,\ldots,N_y-1,$$

$$\hat{S}_{(N_x/2),m} = \hat{S}\left(\frac{\pi}{\Delta_x}, \frac{2\pi m}{N_y\Delta_y}\right), \quad m = 1,2,\ldots,N_y/2,$$

$$\hat{S}_{(N_x/2),N_y-m} = \hat{S}_{(N_x/2),m}, \quad k = N_y/2+1,\ldots,N_y-1,$$

$$\hat{S}_{k,m} = \hat{S}\left(\frac{2\pi k}{N_x\Delta_x}, \frac{2\pi m}{N_y\Delta_y}\right), \quad \begin{cases} k = 1,2,\ldots,N_x/2-1, \\ m = 1,2,\ldots,N_y/2-1, \end{cases}$$

$$\hat{S}_{k,N_y-m} = \hat{S}\left(\frac{2\pi k}{N_x\Delta_x}, -\frac{2\pi m}{N_y\Delta_y}\right), \quad \begin{cases} k = 1,2,\ldots,N_x/2-1, \\ m = N_y/2+1,\ldots,N_y-1, \end{cases}$$

$$\hat{S}_{N_x-k,N_y-m} = \hat{S}_{k,m}, \quad \begin{cases} k = N_x/2+1,\ldots,N_x-1, \\ m = 1,2,\ldots,N_y-1. \end{cases} \tag{A.6}$$

(3) From relation (A.4), the magnitude of the DFT $F_{k,m}$ of the distribution $f(x,y)$ is

$$|F_{k,m}| = \sqrt{\frac{(2\pi)^2}{L_xL_y}\hat{S}_{k,m}}. \tag{A.7}$$

If $\theta_{k,m}$ is a random phase angle chosen from a population with a uniform probability distribution between 0 and 2π, $F_{k,m}$ is thus given by

$$F_{k,m} = \sqrt{\frac{(2\pi)^2}{L_xL_y}\hat{S}_{k,m}}\mathrm{e}^{\mathrm{i}\theta_{k,m}}. \tag{A.8}$$

In choosing the random phase angle $\theta_{k,m}$ in Eq. (A.8), it is required that relation (A.2) is satisfied. So $\theta_{k,m}$ must be chosen following the prescription:

$$\theta_{0,0} = \theta_{(N_x/2),0} = \theta_{0,(N_y/2)} = \theta_{(N_x/2),(N_y/2)} = 0,$$

$$\theta_{k,0} \text{ is random}, \quad k = 1,2,\ldots,N_x/2-1,$$

$$\theta_{N_x-k,0} = -\theta_{k,0}, \quad k = N_x/2+1,\ldots,N_x-1,$$

$$\theta_{0,m} \text{ is random}, \quad m = 1,2,\ldots,N_y/2-1,$$

$$\theta_{0,N_y-m} = -\theta_{0,m}, \quad m = N_y/2+1,\ldots,N_y-1,$$

$$\theta_{(N_x/2),m} \text{ is random}, \quad m = 1,2,\ldots,N_y/2-1,$$

$$\theta_{(N_x/2),N_y-m} = -\theta_{N_x/2,m}, \quad k = N_y/2+1,\ldots,N_y-1,$$

$$\theta_{k,m} \text{ is random}, \quad \begin{cases} k = 1,2,\ldots,N_x/2-1, \\ m = 1,2,\ldots,N_y-1, \end{cases}$$

$$\theta_{N_x-k,N_y-m} = -\theta_{k,m}, \quad \begin{cases} k = N_y/2+1,\ldots,N_x-1, \\ m = 1,2,\ldots,N_y-1. \end{cases} \tag{A.9}$$

(4) The random discrete distribution is given by the inverse DFT of Eq. (A.8):

$$f_{k,m} = \sum_{r=0}^{N_x-1} \sum_{s=0}^{N_y-1} F_{rs} \exp\left(2\pi \mathrm{i}\left(\frac{kr}{N_x} + \frac{ms}{N_y}\right)\right) \quad \begin{cases} k = 0, 1, \ldots, N_x - 1, \\ m = 0, 1, \ldots, N_y - 1. \end{cases} \tag{A.10}$$

The discrete transform (A.10) can be efficiently evaluated by using the fast Fourier transform (FFT) algorithm. The resulting random realisations will be real valued and have zero mean and the specified spectral density. They will also be periodic over the intervals $k = (0, N_x)$ and $m = (0, N_y)$, i.e. $f_{0,m} = f_{Nx,m}$ $(m = 0, 1, 2, \ldots, N_y - 1)$ and $f_{k,0} = f_{k,N_y}$ $(k = 0, 1, 2, \ldots, N_x - 1)$, but it is assumed that this will not affect the results of the Monte Carlo simulation.

References

Argon, A.S., 1972. Fracture of composites. Treatise Mater. Sci. Technol. 1, 79–114.

Budiansky, B., 1983. Micromechanics. Comput. Struct. 16, 3–12.

Budiansky, B., Fleck, N.A., 1993. Compressive failure of fiber composites. J. Mech. Phys. Solids 41 (1), 183–211.

Cebon, D., Newland, D.E., 1984. The artificial generation of road surface topography by the inverse FFT method. Proceedings of the Eighth IAVSD Symposium on the Dynamics of Vehicles on Roads and on Tracks, MIT, Cambridge, MA, 15–19 August, 1983, Swets and Zeitlinger, Amsterdam.

Chen, C., Lu, T.J., Fleck, N.A., 1999. Effect of imperfections on the yielding of two-dimensional foams. J. Mech. Phys. Solids 47 (11), 2235–2272.

Clarke, A.R., Archenhold, G., Davidson, N., Slaughter, W.S., Fleck, N.A., 1996. Determining the power spectral density of the waviness of unidirectional glass fibres in polymer composites. Appl. Compos. Mater. 2, 233–243.

Creighton, C.J., Sutcliffe, M.P.F., Clyne, T.W., 2001. A multiple field image analysis procedure for characterisation of fibre alignment in composites. Composites A 32, 221–229.

Crisfield, M.A., 1991. Non-linear Finite Element Analysis of Solids and Structures, Vol. 1. Wiley, England.

Fleck, N.A., 1997. Compressive failure of fibre composites. Advances in Applied Mechanics, Vol. 33. Academic Press, New York, pp. 43–119.

Fleck, N.A., Liu, D., 2001. Microbuckle initiation from a patch of large amplitude fibre waviness in a composite under compression and bending. Eur. J. Mech. A/Solids 20, 23–27.

Fleck, N.A., Jelf, P.M., 1995. Deformation and failure of a carbon fibre composite under combined shear and transverse loading. Acta Metall. Mater. 43 (8), 3001–3007.

Fleck, N.A., Shu, J.Y., 1995. Microbuckle initiation in fibre composites: a finite element study. J. Mech. Phys. Solids 43 (12), 1887–1918.

Fleck, N.A., Deng, L., Budiansky, B., 1995. Prediction of kink width in compressed fibre composites. J. Appl. Mech. 62, 329–337.

Fleck, N.A., Liu, D., Shu, J.Y., 2000. Microbuckle initiation from a hole and from the free edge of a fibre composite. Int. J. Solids Struct. 37, 2757–2775.

Garland, B.D., Beyerlein, I.J., Schadler, L.S., 2001. The development of compression damage zones in fibrous composites. Compos. Sci. Technol. 61 (16), 2461–2480.

Hsu, S.Y., Vogler, T.J., Kyriakides, S., 1998. Compressive strength predictions for fibre composites. J. Appl. Mech. 65, 7–16.

Jelf, P.M., Fleck, N.A., 1992. Compression failure mechanisms in unidirectional composites. J. Compos. Mater. 26 (18), 2706–2726.

Jelf, P.M., Fleck, N.A., 1994. The failure of composite tubes due to combined compression and torsion, J. Mater. Sci. 29 (3090) 3084.

Jensen, H.M., Christoffersen, J., 1997. Kink band formation in fibre reinforced materials. J. Mech. Phys. Solids 45 (7), 1121–1136.

Kyriakides, S., Ruff, A.E., 1997. Aspects of failure and post failure of fibre composites in compression. J. Compos. Mater. 31, 2000–2037.

Kyriakides, S., Arseculeratne, R., Perry, E.J., Liechti, K.M., 1995. On the compressive failure of fibre reinforced composites. Int. J. Solids Struct. 32 (6/7), 689–738.

Lankford, J., 1995. Compressive failure of fibre-reinforced composites: buckling, kinking and the role of the interphase. J. Mater. Sci. 30, 4343–4349.

Moran, P.M., Liu, X.H., Shih, C.F., 1995. Kink band formation and band broadening in fibre composites under compressive loading. Acta Metall. Mater. 43 (8), 2943–2958.

Newland, D.E., 1984. An Introduction to Random Vibrations and Spectral Analysis, 2nd Edition. Wiley, New York.

Schapery, R.A., 1995. Prediction of compressive strength and kink bands in composites using a work potential. Int. J. Solids Struct. 32 (6/7), 739–765.

Schultheisz, C.R., Waas, A.M., 1996. Compressive failure of composites, Part I: testing and micromechanical theories. Prog. Aerospace Sci. 32, 1–42.

Shu, J.Y., Fleck, N.A., 1997. Microbuckle initiation in fibre composites under multiaxial loading. Proc. Roy. Soc. A 453, 2063–2083.

Slaughter, W.S., Fleck, N.A., 1994. Microbuckling of fiber composites with random initial fiber waviness. J. Mech. Phys. Solids 42 (11), 1743–1766.

Sun, C.T., Chen, J.L., 1989. A simple flow rule for characterizing nonlinear behavior of fiber composites. J. Compos. Mater. 23, 1009–1020.

Sutcliffe, M.P.F., Fleck, N.A., 1994. Microbuckle propagation in carbon fibre-epoxy composites. Acta Metall. Mater. 42 (7), 2219–2231.

Sutcliffe, M.P.F., Yuwono, A.H., 2001. Experimental study of microbuckle initiation in a model composite system. Scr. Mater. 45, 831–837.

Vogler, T.J., Kyriakides, S., 2001. On the initiation and growth of kink bands in fibre composites: Part I. Experiments. Int. J. Solids Struct. 38 (15), 2639–2651.

Vogler, T.J., Hsu, S.Y., Kyriakides, S., 2001. On the initiation and growth of kink bands in fibre composites: Part II. Analysis. Int. J. Solids Struct. 38 (15), 2653–2682.

Waas, A.M., Schultheisz, C.R., 1996. Compressive failure of composites, Part II: Experimental studies. Prog. Aerospace Sci. 32, 1–42.

Wisnom, M.R., 1994. The effect of fibre waviness on the relationship between compressive strength of unidirectional composites. J. Compos. Mater. 28, 66–76.

Yurgatis, S.W., 1987. Measurement of small angle misalignments in continuous fibre composites. Compos. Sci. Technol. 30, 279–293.